JOURNAL OF MATERIALS SCIENCE 11 (1976) 1781–1793

Coupled eutectic growth in Al-Fe alloys

Part 1 *Effects of high growth velocity*

I. R. HUGHES*, H. JONES
Department of Metallurgy, University of Sheffield, St. George's Square, Sheffield, UK

The conditions for fully eutectic growth in Al–Fe alloys at a temperature gradient of 20 K mm^{-1} are reported for ranges of composition from 2.2 to 6.1 wt % Fe and of growth velocity from 0.03 to 10 mm sec^{-1}. All six main classes of growth structure (i.e. Al–Al_3Fe or Al–Al_6Fe eutectics either alone or together with primary αAl or Al_3Fe) were obtained, some of them reported for the first time for steady-state conditions. Observed concentration-dependences both of the limiting growth velocity for primary Al_3Fe and of the interphase spacing for the fully eutectic Al–Al_6Fe displacing it are in good agreement with theory. Hardness levels for the Al–Al_6Fe eutectic as a function of concentration are similar to those for αAl dendritic structures grown in much thinner sections under splat-cooling conditions. The significance of some observed transitions in growth morphology for eutectic cells, Al_6Fe eutectic rods and αAl dendrites is discussed.

1. Introduction

Dix [1] reported as long ago as 1925 that chill casting could result in fully eutectic growth in Al–Fe alloys at iron concentrations well in excess of the eutectic composition of 1.7 wt % Fe. More systematic studies of the effect for the range 1 to 7 wt % Fe by quenching 20 mg alloy droplets into molten sodium at two difference temperatures were reported in 1955 by Scheil and Masuda [2], and in 1958, Towner [3] showed that atomization suppressed hypereutectic growth of Al_3Fe at concentrations as high as 7.6 wt % Fe. Hollingsworth *et al.* [4] in 1962 discovered the formation of metastable Al_6Fe partially displacing equilibrium Al_3Fe in continuously cast Al–2 wt % Fe, and in 1968 Bäckerud [5] reported controlled cooling studies for the range 0.5 to 4 wt % Fe indicating that a cooling rate threshold of 3 K sec^{-1} had to be exceeded to displace the equilibrium Al–Al_3Fe eutectic by that of metastable Al–Al_6Fe. Tonejc and Bonefačić [6] and Jones [7] in 1969 reported the formation of Al_6Fe by splat-cooling ($\sim 10^6$ sec^{-1}) at concentrations as high as 20 wt % Fe, and Burden and Jones [8] in 1970 showed the range of possible growth structures in wedge-section chill castings for concentrations between 1.3 and 11 wt % Fe. Subsequent work by Adam *et al.* [9–12] extended the controlled cooling studies of Bäckerud and additionally employed steady-state solidification at growth velocities up to 2 mm sec^{-1} to define the growth conditions and morphology of the two eutectics for 2 to 4 wt % Fe. The present work extends these studies to higher concentrations and growth velocities and reports on the effect of growth conditions on hardness. A further paper [13] will report on the thermal stability of the Al–Al_6Fe eutectic grown under these conditions.

2. Experimental

Alloys containing 2.2 to 6.1 wt % iron were prepared from super-purity aluminium ($\sim$ 99.99%) and a master alloy containing 40 wt % iron made from the same aluminium and Japanese electrolytic iron ($\sim$ 99.9% pure). Melting was carried out in alumina crucibles in 2 kg capacity vacuum melting equipment, casting under argon into steel chill moulds to produce ingots 25 mm diameter by 150 mm long. These were hot-rolled at 720 to 870 K to 10 mm diameter to allow swaging to 6.5 mm and final drawing to 3.2 or 1.6 mm diameter with intermediate anneals at 870 K.

* Present address: Alcan International Ltd, Banbury, Oxon, UK.

Lengths of alloy rod were induction-melted and longitudinally solidified in graphite crucibles in apparatus similar to that described by Cline and Livingston [14]. Steady solidification at speeds selected from 70 in the range 5.1×10^{-5} to 41 mm sec^{-1} was achieved by employing a ten-speed synchronous motor with a stepped drive shaft serving as a winch. Alloys were r.f.-melted in a graphite crucible screwed to the top of vertical brass withdrawal rod attached to the winch by a length of steel cord. A bath of circulating water immediately below the r.f. melting coil and graphite susceptor ensured a temperature gradient of 20 K mm^{-1} during withdrawal of the brass rod and crucible through it. As found previously [14], solidification became radial at high withdrawal speeds, occurring for our conditions above 4 mm sec^{-1} for crucibles of 6 mm external diameter. Hence crucibles of 3 mm external diameter were used for the range 4 to 12 mm sec^{-1}. Specimens were 90 mm long by 3.2 mm diameter in the larger crucible and 50 mm long by 1.6 mm diameter in the smaller one. Transient effects were completed within the initial 10 mm of solidification.

Longitudinal and transverse sections of solidified rods were prepared for optical microscopy by polishing to 1 μm diamond finish followed by electrolytic polishing at 0° C in a solution of perchloric acid and ethylene glycol monobutyl ether in methanol in the proportions 6:35:59 by volume [15]. For scanning electron microscopy, this was followed by deep etching in 5% NaOH solution. Discs 3 mm diameter and 0.25 mm thick cut from specimen rods were prepared for transmission electron microscopy by electrolytic dishing from both sides in 20% perchloric acid/methanol solution followed by electrolytic perforation at $-70°$ C in 10% perchloric acid/methanol. X-ray diffractometry with CoKα radiation was carried out on filings. Vickers hardness measurements were the average of ten indents on longitudinal sections. Microhardness measurements were the average of fifteen indents on transverse sections.

3. Results

3.1. Regimes of growth

Dominant growth structures as a function of growth velocity V and alloy concentration are indicated in Fig. 1. All six main classes of expected growth constitution, namely eutectics Al–Al_3Fe (EU1) and Al–Al_6Fe (EU2) either alone or together with primary αAl or Al_3Fe, were observed within the range of conditions studies. Figs. 2 to 4 contrast the structures of the two eutectics occurring alone (Fig. 2a and b), with αAl (Fig. 3a and b), and with Al_3Fe (Fig. 4a and b).

The eutectics were readily distinguished by the regular rod morphology of EU2 (Fig. 2a) compared with the irregular plate form of EU1 (Fig. 2b) and by the lower and higher proportion, respectively, of EU2 compared with EU1 for hypoeutectic (Fig. 3a and b) and hypereutectic (Fig. 4a and b) structures. Structures involving EU1 were displaced by those containing EU2 at velocities exceeding ~ 0.1 mm sec^{-1} practically independent of alloy concentration. EU1 with or without αAl was observed only at iron contents

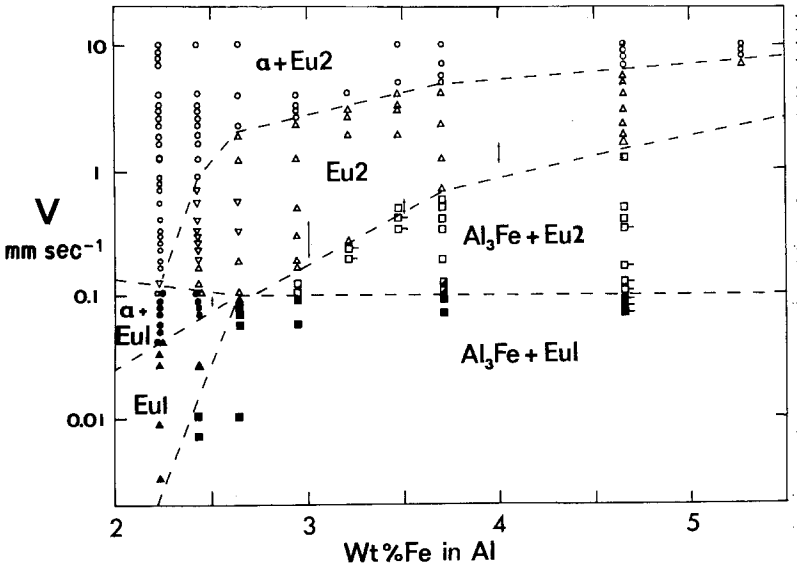

Figure 1 Dominant growth morphologies as a function of growth velocity V and alloy concentration in Al–Fe alloys solidified with a temperature gradient of 20 K mm^{-1}. EU1 = Al–Al_3Fe eutectic, EU2 = Al–Al_6Fe eutectic, α = dendritic αAl solid solution. Inverted open triangles indicated presence of incipient αAl dendrites shown in Fig. 6a. Square with side tag indicate pronounced αAl halo-formation around primary Al_3Fe dendrites. Half-filled squares indicate mixed EU1/EU2 matrix surrounding primary Al_3Fe dendrites. Double headed arrows indicate results of Adam and Hogan [9] for the upper limiting velocity for primary Al_3Fe growth in competition with fully eutectic EU2.

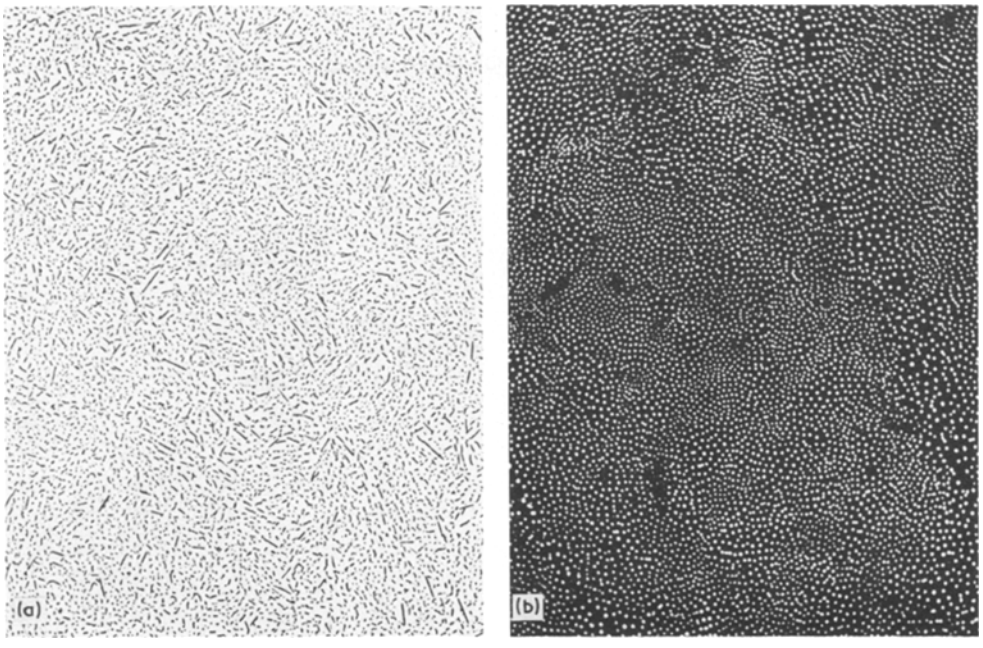

Figure 2 Comparison of morphologies of $Al-Al_3Fe$ and $Al-Al_6Fe$ eutectic growth. (a) $Al-Al_3Fe$, 2.2 wt % Fe, 9.1×10^{-3} mm sec^{-1}. Optical micrograph × 100. (b) $Al-Al_6Fe$, 2.4 wt % Fe, 8.1×10^{-1} mm sec^{-1}. Scanning electron micrograph × 1800. Both etched transverse to growth direction.

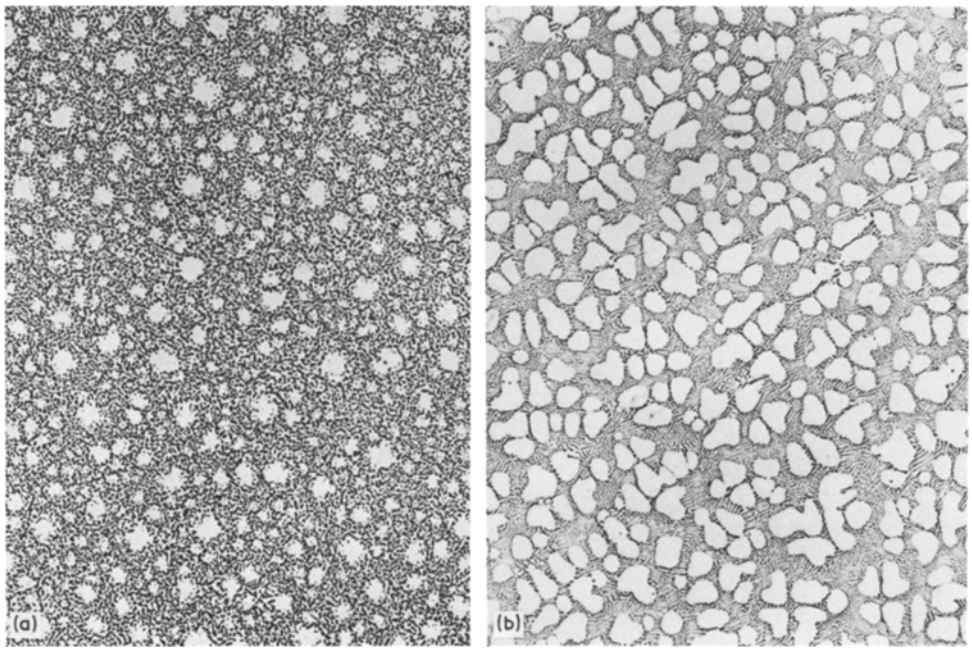

Figure 3 Primary αAl dendritic growth in Al–2.2 wt % Fe with eutectics of (a) $Al-Al_3Fe$ at 7.1×10^{-2} mm sec^{-1}, × 130; and (b) $Al-Al_6Fe$ at 2.7×10^{-1} mm sec^{-1}, × 290. Both optical micrographs of etched transverse sections.

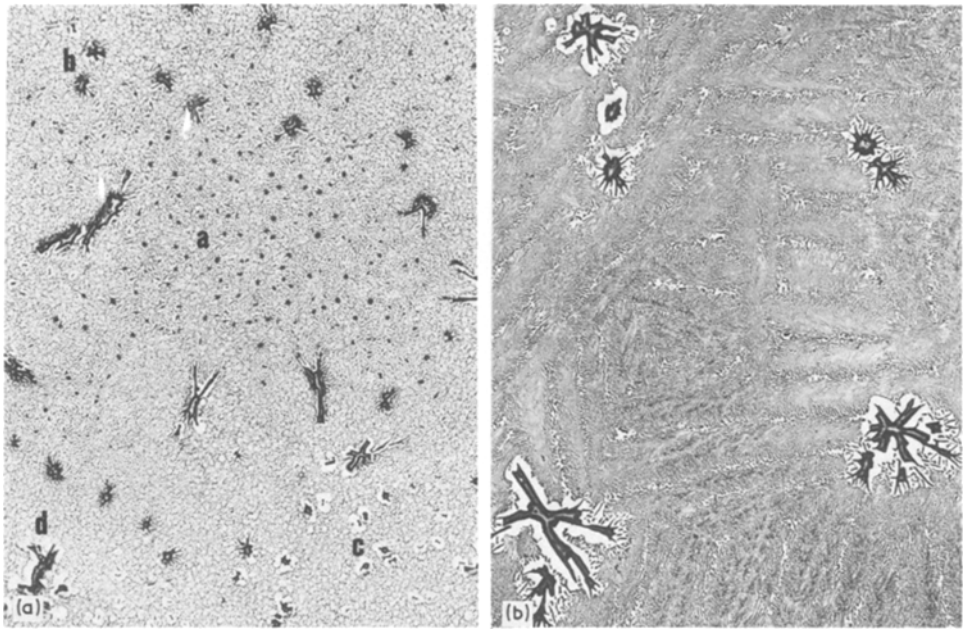

Figure 4 Primary Al_3Fe growth in Al–3.7 wt% Fe with eutectics of (a) Al–Al_3Fe at 9.1×10^{-2} mm sec^{-1}, ×50; (b) Al–Al_6Fe at 1.9×10^{-1} mm sec^{-1}, ×130. Both optical micrographs of etched transverse sections.

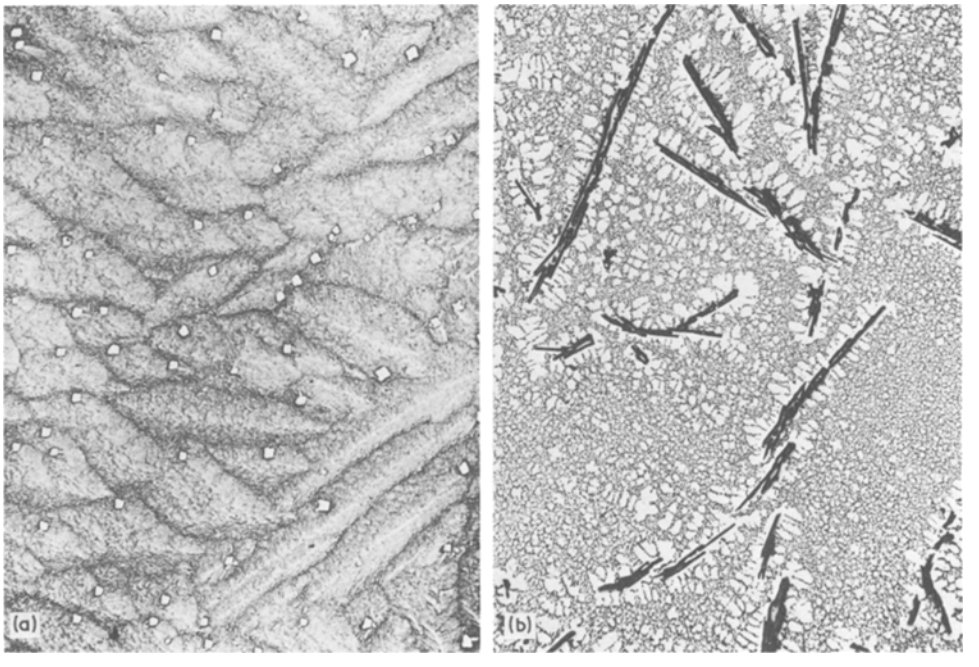

Figure 5(a) Incipient αAl primary growth in Al–Al_6Fe eutectic. 2.6 wt% Fe, 3.4×10^{-1} mm sec^{-1}, ×110. (b) Haloes of αAl primary growth around Al_3Fe dendrites. 4.7 wt% Fe, 1.05×10^{-1} mm sec^{-1}, ×40. Both optical micrographs of transverse sections.

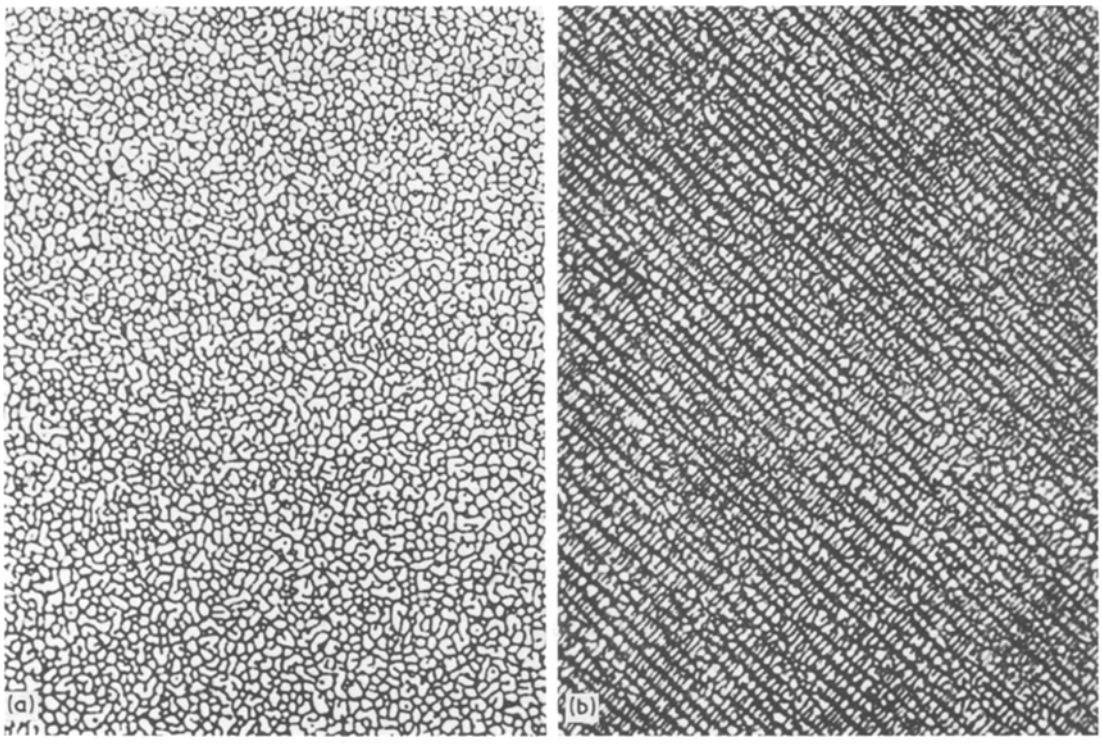

Figure 6 Effect of alloy concentration on morphology of αAl dendritic growth at high V, (a) rod-like growth for 2.6 wt % Fe, × 700; (b) plate-like cellular-dendritic growth for 6.1 wt % Fe, × 1200. Both optical micrographs of transverse sections for V of 10.5 mm sec^{-1}.

less than 2.7 wt % while EU2 with or without αAl occurred over the entire composition range studied (2.2 to 5.3 wt % Fe). EU2 grown at 2.4 and 2.7 wt % Fe contained what appeared to be incipient αAl dendrites (Fig. 5a) except at the highest and lowest velocities in the phase field, while Al_3Fe dendrites were subject to pronounced αAl halo formation at the higher growth velocities employed for 3.2 and 3.4 wt % Fe and at lower growth velocities for 4.7 wt % Fe (Fig. 5b). Fig. 6a and b show the tendency for the rod-like αAl dendritic growth form preferred at high V to become more branched and plate-like at higher concentration.

Fig. 7 illustrates the sensitivity of hardness (H_V) measurements to changes in growth regime with increasing growth rate. The steeper increase in H_V when Al_3Fe growth is fully displaced by EU2 and the sharp decrease in H_V at high V when αAl growth displaces EU2 are both very evident.

3.2. Microstructural features and hardness of EU2

The Al–Al_6Fe eutectic grew as arrays of plate-like cells (Fig. 8a) becoming less regular with decreasing growth rate. Transverse bands reflecting longitudinal fluctuations in Al_6Fe rod density and morphology [15] were also observed within cells particularly at lower growth rates (Fig. 8b). An increased tendency towards linking of rods was evident at lower growth rates (Fig. 9a) and higher concentrations (Fig. 9b). Repeated branching of

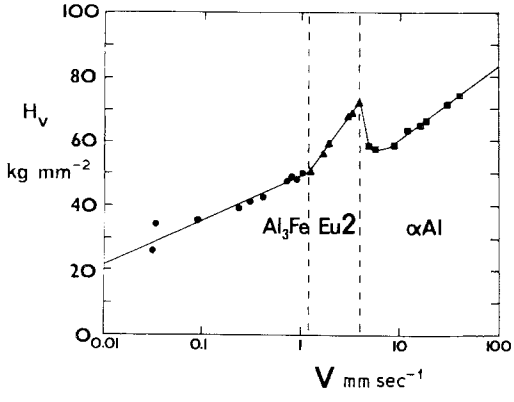

Figure 7 Vickers hardness H_V ($2\frac{1}{2}$kg load) as a function of growth velocity V for 3.6 wt % Fe showing effects of regime of growth operative.

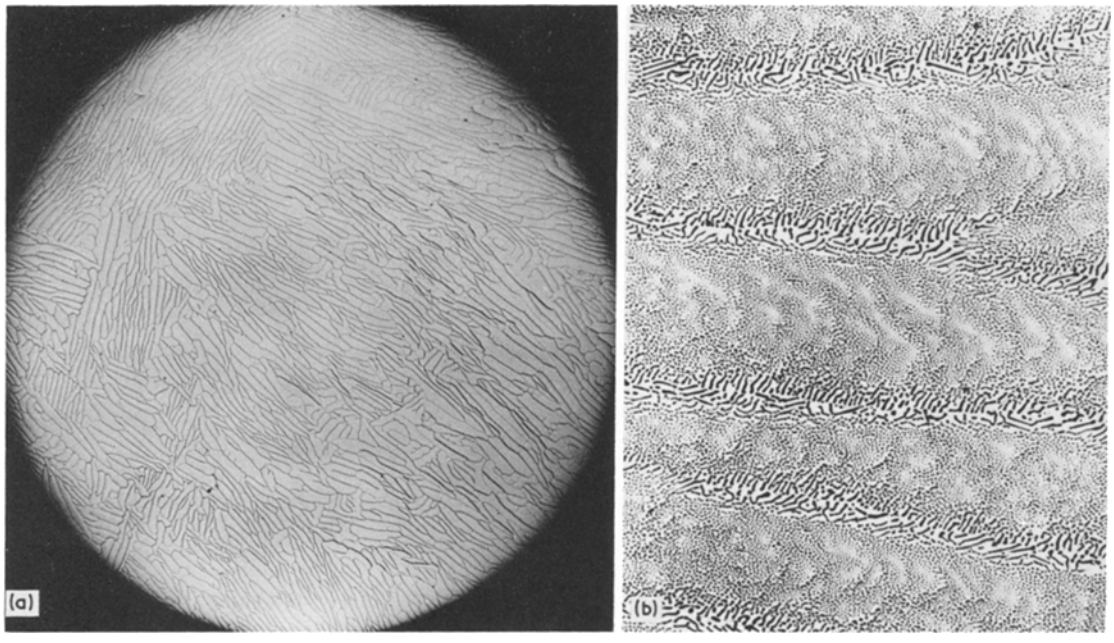

Figure 8(a) Al–Al_6Fe eutectic plate-like cell morphology formed at high V (1.9 mm sec^{-1}, × 26. (b) Transverse banding of Al_6Fe rods within Al–Al_6Fe eutectic cells 1.9×10^{-1} mm sec^{-1}, × 380. Both optical micrographs of transverse sections for 2.6 wt % Fe.

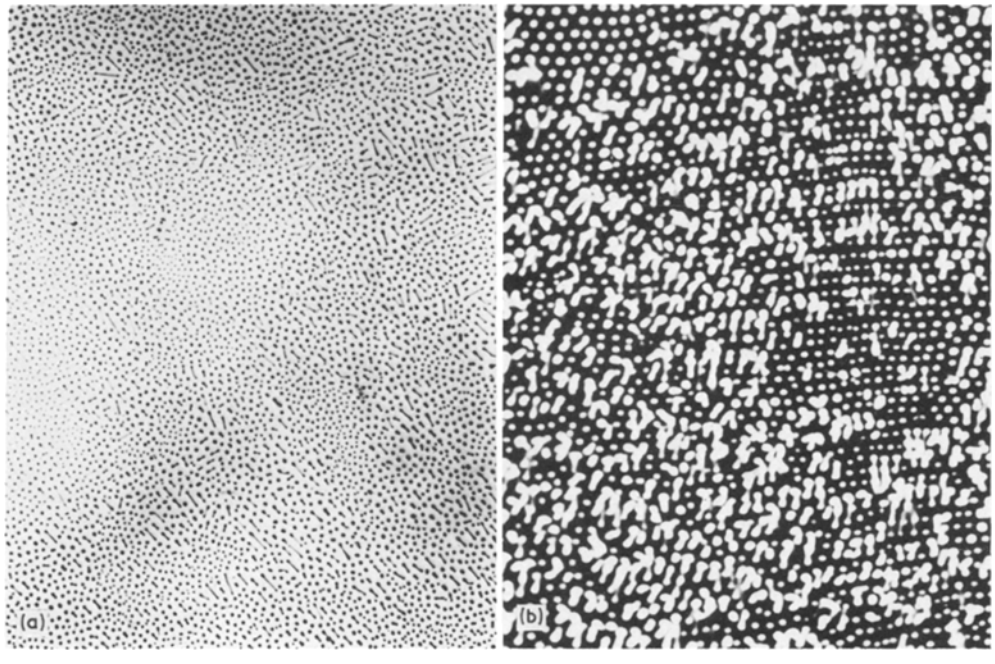

Figure 9 Increased linking of Al_6Fe eutectic rods at high V. (a) Optical micrograph for 2.6 wt % Fe, 0.105 mm sec^{-1}, × 570. (b) Scanning electron micrographs for 3.7 wt % Fe, 4.1 mm sec^{-1}, × 9500. Both etched transverse sections.

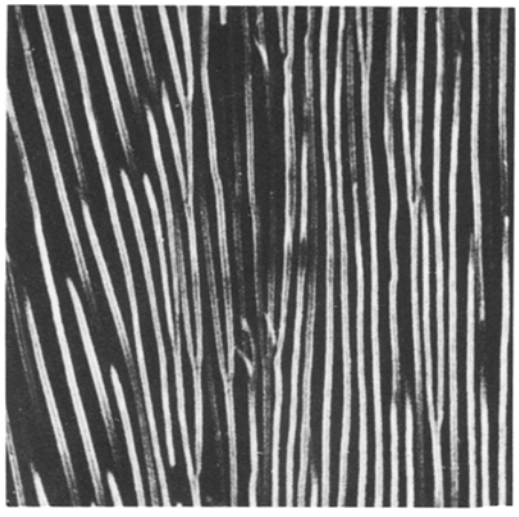

Figure 10 Branching of Al_6Fe rods in Al–Al_6Fe eutectic, 3.0 wt % Fe, 1.2 mm sec^{-1}. Scanning electron micrograph of etched section parallel to growth direction, × 7100.

Al_6Fe rods was evident in scanning electron micrographs of deeply etched longitudinal sections (Fig. 10). Cell thickness and eutectic inter-rod spacing decreased by 50% and 30%, respectively, with increased concentration from 2.6 to 5.3 wt % Fe (Fig. 11). Cell thicknesses were typically 100 times the Al_6Fe rod spacing. The increases in hardness with growth rate and with concentration are shown in Fig. 12a and b for 3.7 wt % Fe and for 1.9 mm sec^{-1} respectively. Fig. 12b also includes, for comparison, results for non-steady-state non-eutectic

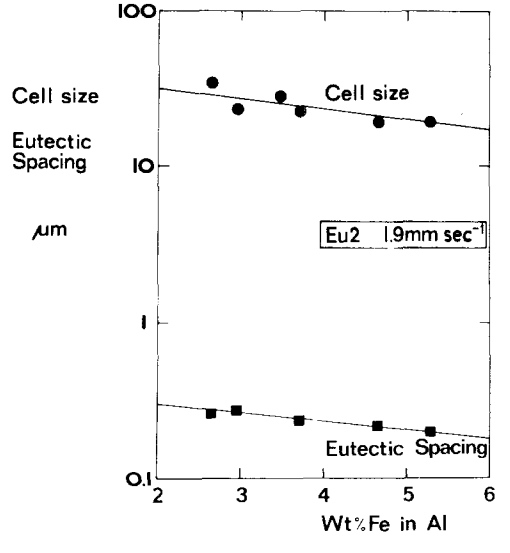

Figure 11 Al–Al_6Fe eutectic cell thickness and interphase spacing as a function of alloy concentration for 1.9 mm sec^{-1}.

growth structures produced in these alloys by splat-cooling and chill casting [7]. EU2 containing 3.6 wt % Fe grown at 2.4 mm sec^{-1} with a Vickers hardness (1 kg load) of 56 kg mm^{-2} was readily worked by wire-drawing or swaging at room temperature to true strains ϵ_t of at least 2.4, producing increases of hardness up to a level of 90 kg mm^{-2} at $\epsilon_t > 1.5$. Continuing hardening up to strains as high as 4.5 found for eutectoid Fe–Fe_3C (e.g. [16]) thus did not occur for eutectic Al–Al_6Fe presumably reflecting the increased recovery possible at $T_M/3$ for aluminium compared with $T_M/6$ for iron.

4. Discussion

4.1. Boundaries of growth regimes

The results in Fig. 1 can be compared with those of controlled cooling experiments on Al–Fe alloys [5, 9] and of similar high velocity steady state growth studies in Al–Fe [9] and other aluminium alloy systems [17–19]. Bäckerud [5] determined a threshold cooling rate of 3 K sec^{-1} to be exceeded to form interdendritic EU2 instead of EU1 in Al–1 wt % Fe and Adam and Hogan [9] obtained the same value for Al–2 wt % Fe. The threshold growth velocity of ~ 0.1 mm sec^{-1} required to displace EU1 by EU2 at a temperature gradient of 20 K mm^{-1} corresponds to a threshold cooling rate of 2 K sec^{-1} for the range 2.2 to 4.7 wt % Fe, in reasonable agreement with the earlier estimates for lower concentrations.

The upper limit of growth velocity for primary Al_3Fe as a function of concentration is also in good agreement with the results of Adam and Hogan; their limits are a factor of 1 to 2 higher than ours for the more limited range 2.5 to 4 wt % Fe they covered. Adam and Hogan did not report observation of αAl growth and the lower limit of growth velocity for αAl formation is thus reported here for the first time. These limits are also comparable with corresponding results for the isomorphous Al–Al_6Mn eutectic [19]. A graph of growth velocity against wt % Mn or Fe or vol % Al_6Mn or Al_6Fe (Fig. 13) shows close agreement except for a considerably extended range of Al–Al_6Fe eutectic growth at high velocities and alloy concentrations.

The systematic trend from a range of coupled eutectic growth asymmetrically displaced to higher concentrations only for Al–Fe (Fig. 12) and Al–Co [17] to a range more symmetrically disposed on both sides of the eutectic composition for Al–Ni

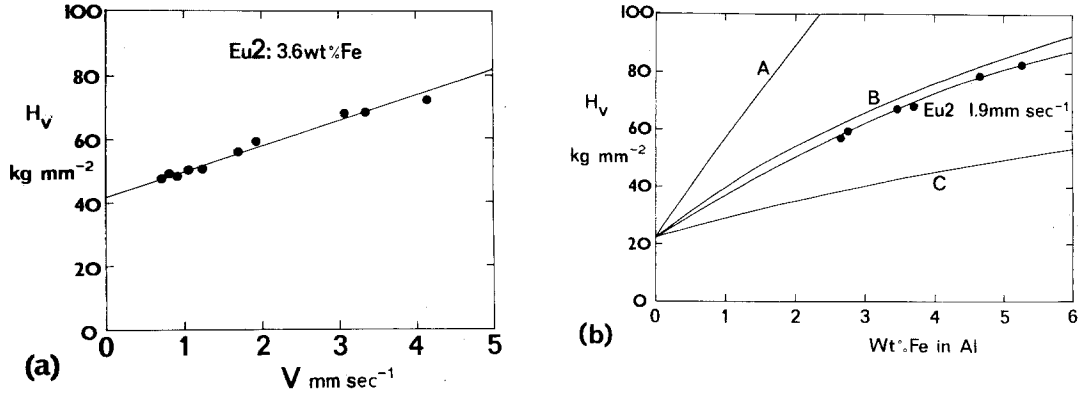

Figure 12 Hardness H_V of Al–Al_6Fe eutectic (a) Vickers hardness (5 kg load) as a function of growth velocity V for 3.6 wt % Fe, and (b) microhardness (100 g load) as a function of alloy concentration in wt % Fe at 1.9 mm sec^{-1} compared with reported data [7] for αAl dendritic growth structures formed by splat cooling (curves A and B) and a range of structures formed by chill casting (curve C).

[17] and Al–Cu [20–23], is in keeping with the following established trends with advancing position of the alloying addition along each transition series:

(i) peritectic to eutectic equilibrium [24];

(ii) decreasing peritectic/eutectic temperature and associated increasing volume function of intermetallic at the eutectic composition [24];

(iii) increasing melting point, density, heat of formation and hardness of the intermetallic phase [25].

Theoretical predictions of the conditions for coupled eutectic growth have been compared with experimental results only for displacement of α–Sn

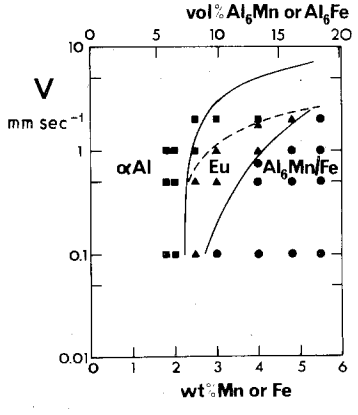

Figure 13 Comparison between limiting conditions for fully eutectic growth of Al–Al_6Fe and Al–Al_6Mn. Full lines indicate the boundaries for Al–Al_6Fe growth from Fig. 1. The dashed line indicates the upper limit of growth velocity for Al–Al_6Mn growth from [19]. The lower limit is indistinguishable from that for Al–Al_6Fe. Experimental points are for Al–Al_6Mn from [19].

dendrites by coupled eutectic growth at hypoeutectic compositions close to the Sn–Pb eutectic composition [26–31]. The best agreement with experiment was obtained by a competitive growth approach [31] yielding:

$$C = C_{EU} + (1/m_3)\,[GD/V + (B' - A')\,C^{1/2}V^{1/2}/D^{1/2}] \qquad (1)$$

where C defines the limiting composition for coupled eutectic growth at velocity V, C_{EU} is the eutectic composition, G is the temperature gradient, D is solute diffusion coefficient in the liquid, m_3 is the liquidus slope for the dendritic phase and B' and A' are defined in Appendix 1. Although direct data for C_{EU}, B' and A', known for Sn–Pb, are not available for Al–Al_6Fe, the results of Figs. 1 and 13 can be employed together with theoretical estimates of A' and B' to estimate C_{EU} and m_3 (see Appendix 1). For the more reliable limit of competition between EU2 and dendritic Al_3Fe growth, a graph of C against $[GD/V + (B' - A')\,C^{1/2}V^{1/2}/D^{1/2}]$ (Fig. 14) yields, from the slope, an m_3 of 12 K/at.% compared with 50 K/at.% from Al_3Fe liquidus determinations [32] and, from the C-intercept, a eutectic composition for Al–Al_6Fe of 1.1 at.% Fe. This is consistent with 0.95 at.% Mn for the Al–Al_6Mn eutectic [5, 19] and identical with the lowest level of 1.1 at.% Fe at which fully eutectic Al–Al_6Fe was grown in the present experiments. The major velocity-dependent term in Equation 1 turns out to be $B'\,C^{1/2}V^{1/2}/D^{1/2}$ in this case. Neither A' or GD/V amount to more than 10% of B' or of

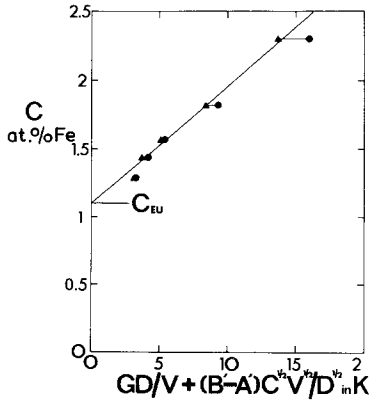

Figure 14 Graph of alloy composition C (at. % Fe) against $[GD/V + (B' - A')\, C^{1/2}V^{1/2}/D^{1/2}]$ in K for the lower velocity limit of fully eutectic growth of Al–Al_6Fe. Each pair of experimental points indicate the lowest V at which growth was fully eutectic and the highest V at which primary Al_3Fe was evident.

$(B' - A')\, C^{1/2}V^{1/2}/D^{1/2}$ respectively over the composition range covered. Burden and Hunt [31] found that better agreement with results for Sn–Pb was obtained when the numerical factor of $2\sqrt{2}$ in B' (see Appendix 1) was increased to 4.5. This would reduce the discrepancy between experimental and predicted slopes for Fig. 14 to a factor of three. This value and the predicted linearity of Fig. 14 within experimental error, indicates reasonable agreement with the theory considering that most of the materials parameters involved in calculating B' are necessarily only estimates. No experimental data corresponding to that for αSn dendrites in Sn–Pb alloys are available for the dependence on growth velocity of growth temperature for an intermetallic such as Al_3Fe. It is also notable that *both* phases in the eutectic differ from the competing dendritic phase in the present case unlike the situation for Sn–Pb where the dendritic phase is also one component of the eutectic.

4.2. Morphology within growth regimes

4.2.1. Effect of V on eutectic cell morphology

Longitudinal eutectic cells in directionally frozen lamellar eutectic such as Al–Al_2Cu tend to be plate-like at low V with the wider of the transverse faces of the plate nearly normal to the eutectic lamellae persisting even with the increasing tendency to form a more equi-axed cell cross-section at increased growth rates [33]. A similar tendency was reported for fibrous Al–Al_3Ni in the same study but more variations in cell shape were apparent between different grains. Nothing corresponding to the very plate-like eutectic cells observed in Fig. 8a for fibrous Al–Al_6Fe at high V seems to have been reported for Al–Al_3Ni, but the decreased regularity of the cell structure at decreased V could correspond to the increased degeneracy of eutectic colonies reported for increased V/G at low V [34]. Such a range of instability at intermediate values of V is an established prediction of interface instability theory [35] used, for example, as an alternative to competitive growth to explain coupled eutectic growth and high and low V [30], and equally applicable in principle to degeneration of cellular growth. This expectation of a more regular cellular morphology at high V is, of course, quite independent of crystallographic considerations governing the tendency for wide faces of plate-like cells in lamellar eutectics to orient preferentially with respect to the interface orientation of lamellae. The elongated cells of Fig. 8a are a well-known stage of interface breakdown in dilute binary alloys (e.g. [36]) for which the wide faces have no crystallographic significance.

4.2.2. Effect of alloy concentration on eutectic cell thickness and interphase spacing

Although the effect of ternary additions on binary eutectic cell size has been reported, (e.g. [37]), no measurements appear to be available for the effect of binary concentration. The 50% decrease in cell thickness with increase in concentration from 2.6 to 5.3 wt % Fe corresponds to the decrease of 30% in interphase spacing λ over the same range. This effect on λ has been studied by Jordan and Hunt [23] for Sn–Pb and Al–Al_2Cu coupled growth at low V. They found that $\lambda^2 V$ decreased by 5% with increased concentration from 32 to 38 wt % Pb in Sn–Pb while exhibiting a maximum at 32 wt % Cu for Al–Al_2Cu (eutectic compositions 37 wt % Cu). The results for Sn–Pb were consistent with theory [38] fitted to the result for 38 wt % Pb (the eutectic composition). Theory [38] predicts

$$\lambda^2 V = B'' D/C \qquad (2)$$

where B'' is defined in Appendix 2. Employing the same values for parameters given in Appendix 1 for calculating the effect of alloy concentration on the limiting condition for primary Al_3Fe growth, gives values of λ typically 10 to 18%

lower than the experimental values plotted in Fig. 11. Thus a fit to within ± 4% of the measured λ is obtained, except for the low experimental λ for 2.6 wt % Fe, by increasing B'' or D in Equation 2 by a factor of 1.3, well within the accuracy with which B'' can be calculated or to which D has been measured in this case.

4.2.3. Morphologies of the Al–Al_6Fe eutectic

Little information is available about the fault structure of fibrous eutectics. Smartt and Courtney [39], however, observed branching and linking of Al_3Ni rods in the Al–Al_3Ni eutectic, similar to our observations for Al–Al_6Fe in Figs. 9 and 10 even at their relatively low growth rates (8×10^{-3} to 3×10^{-2} mm sec^{-1}). They suggest that this linking of rods is a precursor to the development of a plate-like morphology at decreasing growth rates. Our observations confirm that linking is increased at low V and also at high iron contents. The transition from rod-like to lamellar growth with decreasing V is well-documented (e.g. see [40] for references) and stabilization of lamellar growth with increasing volume ratio of the minor to the major phase is as expected, for example, on grounds of decreased total interfacial energy [41]. On the assumption that the stable morphology is the one that will grow at a smaller undercooling, rods are predicted [38] to be stable when $f_2 < 1/\pi = 0.32$ for isotropic interfacial energy. A transition within the range of $0.16 > f_2 > 0.08$ would require minimum anisotropies in Al/Al_6Fe interfacial energy σ_{12} of 9 to 18% according to this approach (see Appendix 3), well within the range of possible anisotropies of solid–solid and solid–liquid interfacial energies [42].

4.2.4. Morphologies of primary αAl and Al_3Fe

The observation (Fig. 6a) of rod-like αAl dendritic growth at the high velocities employed to suppress wholly eutectic or primary Al_3Fe growth, is in agreement with observations for solidification at high cooling rates (e.g. [43, 44]). The stabilization of a more cellular-dendritic form at higher iron contents is attributable to the expected effect of increased constitutional supercooling in promoting more branching during growth. Increased αAl halo formation at lower growth velocities (Fig. 5b) could be a result of increased primary spacing of Al_3Fe dendrites leading to increased isolation of local diffusion fields in surrounding liquid denuded of iron. Increased initial growth of a sheath of αAl is then necessary until this reaches liquid of high enough iron content to be within the regime of coupled eutectic growth for the longitudinal growth velocity applied [45].

4.3. The hardness of Al–Al_6Fe eutectic

The increased hardness with increasing concentration shown in Fig. 12b for coupled Al–Al_6Fe eutectic has also been obtained for Al–Al_3Ni [17, 46]. In the present case, there is an evident correspondence (Fig. 12b) between the level and concentration dependence of hardness of Al–Al_6Fe eutectic grown at 1.9 mm sec^{-1} and those of "zone B", an αAl-dendritic microstructure grown by splat-cooling [7]. It is notable that a cooling rate during solidification of $\sim 10^5$ to 10^6 K sec^{-1} was necessary to produce the *dendrite* cell size ~ 0.3 μm typical of zone B, limiting it to thin sections ($\lesssim 0.1$ mm thick). EU2, of similar hardness, however, can be directionally grown or chill-cast at cooling rates of 10 to 100 K sec^{-1} in sections a few mm thick, with a *eutectic* interphase spacing $\lambda \sim 0.2$ μm, similar to the *dendrite* cell size in zone B. The expectation of an increased hardness in EU2 compared with dendritic αAl grown under the *same* conditions is substantiated in Fig. 7 by the sharp drop in H_V when growth of EU2 is displaced by αAl dendritic growth at $V > 5$ mm sec^{-1} for Al–3.6 wt % Fe. The increased hardness with increasing V at fixed composition (Figs. 7 and 12a) accords with results of Barclay *et al.* [17] and Kurilo *et al.* [47] for the Al–Al_3Ni eutectic. There was no indication of a maximum followed by an eventual decrease in H_V with increasing V attributed [48, 49] to the appearance of eutectic cells. Chadwick [50] has warned against attributing particular significance for eutectics to parametric relationships of H_V with λ, as, for example, given by a Hall–Petch type of relation. Davies and Hellawell [51] showed that a substantial part of hardening in Al–Al_2Cu lamellar eutectic at high V resulted from associated higher cooling rates through the solid state following solidification. These higher cooling rates would be expected to generate thermal stresses [50] and solute supersaturation [51] in suitable systems. Such effects may, in principle, be removed by subsequent heat treatment, the results of which are reported in the companion paper [13].

5. Conclusions

(1) Fully eutectic Al–Al_6Fe growth over the composition range 2.6 to 5.3 wt % Fe, is stable in competition with αAl dendritic growth to higher growth velocities than for the isomorphous Al–Al_6Mn eutectic [19].

(2) The dependence on alloy concentration of limiting growth velocity for primary Al_3Fe in competition with fully eutectic Al–Al_6Fe, agrees to within a factor of three with predictions based on competitive growth and is consistent with a eutectic composition of 1.1 at. % (2.2 wt %) Fe for Al–Al_6Fe.

(3) The stabilization of regular plate-like eutectic cellular growth for Al–Al_6Fe at high V accords with the expectation of a range of interface instability (degeneracy) at intermediate V.

(4) Measurements of Al–Al_6Fe eutectic interphase spacing λ decreasing with increasing alloy concentration, parallel to its effect on eutectic cell size, are within 20% of those predicted by theory [38]. Indications of a transition from rod-like to plate-like growth in the eutectic with increasing alloy concentration from 2.4 to 4.7 wt % Fe are consistent with an effective anisotropy of Al/Al_6Fe interfacial energy of 9 to 18%.

(5) The attainment of hardness levels in Al–Al_6Fe rod eutectic, equal to those of αAl dendritic structures grown in much thinner sections and at higher cooling rates, reflects the smaller interphase spacing attainable under the same solidification conditions for fully eutectic compared with αAl dendritic growth.

Appendix 1. Parameters governing competitive growth between Al–Al_6Fe eutectic and primary Al_3Fe

The parameters A' for the eutectic phases 1 and 2 and B' for the dendritic phase 3 for the critical condition governing coupled eutectic growth given by Equation 1 are defined as:

$$A' = 4\sqrt{2m}\left\{(1+\zeta)^{3/2}\left(1+\frac{a_1}{a_2}\cdot\frac{m_2}{m_1}\cdot\frac{1}{\zeta}\right)\frac{M}{\zeta}\cdot\frac{a_2}{m_2}\right\}^{1/2} \quad \text{(A1)}$$

and $$B' = 2\sqrt{2}\{\sigma_3(T_3/L_3)(1-k_3)m_3\}^{1/2} \quad \text{(A2)}$$

where

$$a_i = (T_i/L_i)\,\sigma_i \sin\theta_i, \; m = \left(\frac{1}{m_1}+\frac{1}{m_2}\right)^{-1}$$

and T_i, L_i and m_i are liquidus temperature, latent heat and liquidus slope of phases 1, 2 and 3; σ_i and θ_i are interfacial energy and inclination to the plane of the growth front of the interface between phase 1 or 2 and the melt; k_3 is the partition coefficient of phase 3 with respect to the liquid phase; ζ is the volume ratio of the major phase 1 to the minor phase 2 in the eutectic, and M is a function of ζ [39, 52]. In the present case, phases 1, 2 and 3 are identified with αAl, Al_6Fe and Al_3Fe respectively. The following data were employed to evaluate A' and B': m_1 as 6 K/at. % Fe [53]; m_2 as 50 K/at. % Fe from Al_6Mn liquidus in Al–Mn [54]; σ_2 of 0.093 J m^{-2} [55]; σ_2 as 0.160 J m^{-2} (estimated on basis that molar interfacial energy is 0.5 of the molar heat of fusion [55]: heat of fusion estimated from data for Al and Fe and composition of Al_6Fe [4] and molar volume from density reported by Walford [56]); sin θ_1 and sin θ_2 from σ_1, σ_2 and Al–Al_6Fe eutectic interphase boundary energy σ_{12} assuming equilibrium prevails at the interfacial junction with the melt (σ_{12} taken as 0.225 J m^{-2} [57] from application of theory [38] to measurements of interphase spacing as a function of growth rate for Al–Al_6Fe eutectic). (T_1/L_1) as 8.8×10^{-7} K m^3 J^{-1} for pure Al from handbook data (e.g. [58]): (T_2/L_2) as 6.3×10^{-7} K m^3 J^{-1} from entropy data for Al and Fe [58] and composition of Al_6Fe [4] including a contribution from ordering: (T_3/L_3) as 5.85×10^{-7} K m^3 J^{-1} estimated as for (T_2/L_2) with composition of Al_3Fe from Black [59]: σ_3 as 0.300 J m^{-2} (estimated as for σ_2 from heat of fusion evaluated from (T_3/L_3) and T_3 of 1421 K [60]: σ_3 as 80 K/at. % Fe [32] and k_3 assumed $\ll 1$ [30, 53, 60]: D as 1.5×10^{-9} m^2 sec^{-1} [61, 62].

Appendix 2. Parameters governing Al–Al_6Fe eutectic interphase spacing

The parameter B'' in Equation 2 for the eutectic phases 1 and 2 is defined [38] by:

$$B'' = \phi' a_2^R / m_2$$

and

$$\phi' = \left(1+\frac{a_1^R}{a_2^R}\cdot\frac{m_2}{m_1}\cdot\frac{1}{\zeta}\right)\zeta/[2M\sqrt{(1+\zeta)}]$$

where a_i^R, m_i, ζ and M have the same meanings and values for the Al–Al_6Fe eutectic as are given in Appendix 1.

Appendix 3. Condition for transition from rod-like to lamellar eutectic growth with increased alloy concentration

The condition for stability of rod-like rather than lamellar eutectic growth, according to Jackson and Hunt [38], is

$$\frac{\left(\frac{a_2^L}{m_2}+\frac{a_1^L}{m_1}\right)}{\left(\frac{a_2^R}{m_2}+\frac{a_1^R}{m_1}\right)} > \frac{4M}{P}\cdot\frac{1}{(1+\zeta)^{3/2}}$$

where superscripts L and R refer to terms for lamellae and rods respectively, P is a function of ζ [38, 52], a_i, m_i, ζ and M again have the same significance as in Appendix 1. The anisotropy of σ_{12} required to satisfy this condition for the composition range 2.4 to 4.7 wt % Fe was evaluated in terms of the ratio n equal to $\sigma_{12}^L/\sigma_{12}^R$.* Employing the data for Appendix 1 for Al–Al_6Fe (including σ_{12}^R as 0.225 J m^{-2}), then yields n values of 0.82 and 0.91 for 2.4 and 4.7 wt % Fe respectively.

Acknowledgements

The authors are grateful to Professors G. W. Greenwood and B. B. Argent for providing laboratory facilities and to the Science Research Council for supporting one of us (IRH).

References

1. E. H. DIX, *Proc. ASTM* **25** (1925) 120.
2. E. SCHEIL and Y. MASUDA, *Aluminium* **31** (1955) 51.
3. R. J. TOWNER, *Metal Prog.* **73** (5) (1958) 70.
4. E. H. HOLLINGSWORTH, G. R. FRANK and R. E. WILLETT, *Trans. Met. Soc. AIME* **224** (1962) 188.
5. L. BÄCKERUD, *Jernkont. Ann.* **152** (1968) 109.
6. A. TONEJC and A. BONEFAČIĆ, *J. Appl. Phys.* **40** (1969) 419.
7. H. JONES, *Mater. Sci. Eng.* **5** (1969/70) 1.
8. M. H. BURDEN and H. JONES, *Metallogr.* **3** (1970) 307.
9. C. MCL. ADAM and L. M. HOGAN, *J. Austral. Inst. Met.* **17** (1972) 81.
10. C. MCL. ADAM, I. O. SMITH and L. M. HOGAN, in Proceedings of the 1972 Lakeville Conference on *In Situ* Composites Vol. II, National Materials Advisory Board 1973 (NMAB 308-II).
11. A. J. MCLEOD, L. M. HOGAN, C. MCL. ADAM and D. C. JENKINSON, *J. Crystal Growth* **19** (1973) 301.
12. C. MCL. ADAM and L. M. HOGAN, *Acta Met.* **23** (1975) 345.
13. I. R. HUGHES and H. JONES, *J. Mater. Sci.* to be published.
14. H. E. CLINE and J. D. LIVINGSTON, *Trans. Met. Soc. AIME* **245** (1969) 1987.
15. H. B. SMARTT and T. H. COURTNEY, *Met. Trans.* **4** (1973) 217.
16. J. D. EMBURY and R. M. FISHER, *Acta Met.* **14** (1966) 147.
17. R. S. BARCLAY, H. W. KERR and P. NIESSEN, *J. Mater. Sci.* **6** (1971) 1168.
18. H. A. H. STEEN and A. HELLAWELL, *Acta Met.* **20** (1972) 363.
19. J. A. EADY, L. M. HOGAN and P. G. DAVIES, *J. Austral. Inst. Met.* **20** (1975) 23.
20. I. S. MIROSHNICHENKO, *Russian Met.* **5** (1968) 128.
21. I. S. MIROSHNICHENKO and A. YA. ANDREEVA, *Dokl. Akad. Nauk USSR* **186** (1969) 1140, English Version p. 128.
22. G. PFLEIGER and F. DURAND, *Compt. Rend.* **C271** (1970) 1544.
23. R. M. JORDAN and J. D. HUNT, *Met. Trans.* **2** (1971) 3401, *J. Crystal Growth* **11** (1971) 141.
24. B. B. GULYAEV, Doklady Chemistry **164** (1965) 837.
25. E. R. PETTY, *J. Inst. Met.* **89** (1960–61) 343.
26. J. D. HUNT and K. A. JACKSON, *Trans. Met. Soc. AIME* **239** (1967) 864.
27. F. R. MOLLARD and M. C. FLEMINGS, *ibid* **239** (1967) 1526, 1534.
28. K. A. JACKSON, *ibid* **242** (1968) 1275.
29. H. E. CLINE, *ibid* **242** (1968) 1613.
30. H. E. CLINE and J. D. LIVINGSTON, *ibid* **245** (1969) 1987.
31. M. H. BURDEN and J. D. HUNT, *J. Crystal Growth* **22** (1974) 328.
32. A. G. C. GWYER and H. W. L. PHILLIPS, *J. Inst. Met.* **38** (1927) 467.
33. W. H. S. LAWSON, H. W. KERR and M. H. LEWIS, *J. Crystal Growth* **12** (1972) 209.
34. H. W. WEART and D. J. MACK, *Trans. Met. Soc. AIME* **212** (1958) 664.
35. W. W. MULLINS and R. F. SEKERKA, *J. Appl. Phys.* **35** (1964) 444.
36. G. S. COLE, *Canad. Met. Quart.* **8** (1969) 189.
37. W. M. RUMBALL, *Metallurgia* **78** (1968) 141.
38. K. A. JACKSON and J. D. HUNT, *Trans. Met. Soc. AIME.* **236** (1966) 1129.
39. H. B. SMARTT and T. H. COURTNEY, *Met. Trans.* **3** (1972) 2000.
40. J. A. SPITTLE, *Metallogr.* **6** (1973) 115.
41. D. J. S. COOKSEY, D. MUNSON, M. P. WILKINSON and A. HELLAWELL, *Phil. Mag.* **10** (1964) 745.
42. J. BASTERFIELD, W. A. MILLER and G. C. WEATHERLY, *Canad. Met. Quart.* **8** (1969) 131.
43. P. K. ROHATGI and C. M. ADAMS, *Trans. Met. Soc. AIME* **239** (1967) 1737.

* This procedure attributes the anisotropy *entirely* to σ_{12} in order to obtain a measure of the *effective* required anisotropy of interfacial energy in the absence of data on the anisotropy of σ_1 and σ_2 for Al and Al_6Fe.

44. H. MATYJA, B. C. GIESSEN and N. J. GRANT, *J. Inst. Met.* **96** (1968) 30.
45. M. F. X. GIGLIOTTI, G. A. COLLIGAN and G. L. F. POWELL, *Met. Trans.* **1** (1970) 891.
46. A. S. TORTIKA, A. I. SOMOV and YU. P. KURILO, *Phys. Met. Metallogr.* **38** (1) (1974) 136.
47. YU. P. KURILO, A. I. SOMOV, A. S. TORTIKA and O. V. CHERNYY, *Phys. Met. Metallogr.* **35** (2) (1973) 111.
48. S. DIRNFIELD, F. GROSS and S. NIEDZWIEDZ, in "Quantitative Relations between Properties and Microstructure", edited by D. G. Brandon and A. Rosen (Israel Universities Press, Jerusalem, 1969) p. 235.
49. M. M. FARAG and M. A. TAHA, Proceedings of the 1972 Conference on *In Situ* Composites, National Materials Advisory Board, Washington D.C., Publication NMAB-308-II (1973) p. 297.
50. G. A. CHADWICK, *Met. Sci.* **9** (1975) 300.
51. I. G. DAVIES and A. HELAWELL, *Phil. Mag.* **19** (1969) 1285.
52. J. N. CLARK, J. T. EDWARDS and R. ELLIOT, *Met. Trans.* **6A** (1975) 232.
53. M. HANSEN and K. ANDERKO, "Constitution of Binary Alloys", 2nd Edn (McGraw-Hill, New York, 1958).
54. H. W. L. PHILLIPS, *J. Inst. Met.* **69** (1943) 275.
55. D. TURNBULL, *J. Appl. Phys.* **21** (1950) 1022.
56. L. K. WALFORD, *Acta. Cryst.* **18** (1965) 287.
57. C. MCL. ADAM, *Ph.D.* Thesis, Queensland (1971).
58. K. A. GSHNEIDNER, in "Solid State Physics", edited by F. Seitz and D. Turnbull, Vol. 16 (Academic Press, New York, 1964) p. 275.
59. P. J. BLACK, *Acta. Cryst.* **8** (1955) 43.
60. J. R. LEE, *J. Iron Steel Inst.* **194** (1960), 222.
61. T. TAKAHASHI, A. KAMIO and NGUYEN AN TRUNG, *J. Crystal Growth* **24/25** (1974) 477.
62. M. SUGIYAMA, T. UMEDA and H. KATO *J. Jap. Inst. Light Metals* **24** (1974) 263.

Received 23 March and accepted 6 April 1976.